V International Conference on Particle-based Methods – Fundamentals and Applications
PARTICLES 2017
P. Wriggers, M. Bischoff, E. Oñate, D.R.J. Owen, & T. Zohdi (Eds)

APPLICATION OF CONTINUUM FORMS FOR PREDICTING ELASTIC WAVE PROPERTIES OF BRICK MORTAR SYSTEM

SUMET SUPPRASERT[1], LALITH WIJERATHNE[2], MUNEO HORI[3] AND JIAN CHEN[4]

[1] Earthquake Research Institute
University of Tokyo, Bunkyo, Tokyo 113-0032, Japan
[1]sumet.res@gmail.com, [2]lalith@eri.u-tokyo.ac.jp, [3]hori@eri.u-tokyo.ac.jp

[4] Advanced Institute for Computational Science
RIKEN, Minatoshima-Minami, Kobe 650-0047, Japan
jchen@riken.jp

Key words: continuum forms, regularly packed bricks, predicting elastic wave characteristics, continuumnization

Abstract. We developed three continuum forms for brick structures, predicted the elastic wave characteristics and investigated the range of validity of the predictions. One of the continuum form is based on *continuumnization* by Hori et al. and the other two are based on Taylor series expansion. Both continuumnization and second order Taylor expansion based continuum forms can predict p- and s-wave characteristics accurately for wavelengths larger than 7 times the brick dimensions. The second order Taylor expansion can also predict the r-wave characteristics accurately in the same range of wavelengths. It is demonstrated that the full Taylor series based continuum form can predict the elastic wave properties to a remarkable accuracy for the whole range of frequencies and wave numbers. These predictions will be useful in verification of simulation codes, utilizing FEM for analyzing brick structures and engineering applications like non-destructive testing, vibration control, etc.

1 INTRODUCTION

We propose three equivalent continuum forms for identifying the elastic wave properties of regularly packed brick-mortar systems and apply those to analytically predict the characteristics of elastic waves properties. These analytical predictions can be used in wide range of applications like verification of numerical codes, non-destructive identification of material properties, vibration control, design, etc.

Two approaches are used in deriving continuum forms; *Continuumnization* proposed by Hori et al.[1] and Taylor series expansion. A regularly packed brick mortar system is

idealized as a discrete block spring system. Three continuum forms of governing equations are obtained assuming the existence of smooth and continuous vector fields which can approximate the field variables of the idealized discrete system. Continuumnization utilizes the limiting process to approximate difference operations in the discrete form of the governing equations, while the other two continuum forms approximate the field variables of idealized discrete system using Taylor series expansion. One of the Taylor series based continuum form uses second order Taylor expansion while the other uses the whole Taylor series. The continuum from obtained with the whole Taylor series can predict the elastic wave characteristics up to the smallest meaningful wavelength, while the predictions of the other two are accurate within the wavelengths of engineering applications.

The rest of the paper is organized as follows. The section two presents the derivations of the three continuum forms of equation of motion, and corresponding characteristic equations for predicting wave properties for regularly packed brick mortar systems. The third section investigates the range of applicability of each continuum form. Some concluding remarks are given in the last section.

2 CONTINUUM FORMS FOR REGULARLY PACKED BRICK SYSTEM

As the starting point to derive the three equivalent continuum forms, first the discrete equations of motion for a regularly packed brick mortar system is obtained. The rest of this section presents the derivation of the three continuum forms and the analytical predictions of the elastic wave properties.

2.1 Regularly packed bricks as a discrete system

We idealize a single layer brick wall as a network of rigid rectangular blocks connected with infinitesimally short linear elastic springs, as shown in Fig.1(a). The springs represent elasticity of both the bricks and mortar layers while the domain of each rigid block includes a portion of cement layers so that the domain occupied by the brick mortar system is perfectly tessellated.

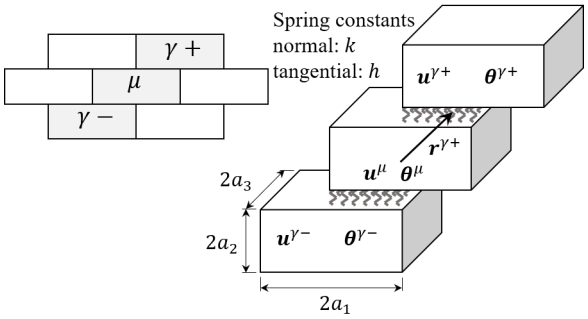

(a) Neighboring blocks of regularly packed bricks

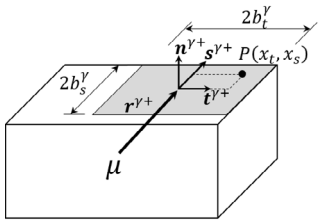

(b) Contact area of two neighboring blocks

Figure 1: Idealized block-spring model.

Consider an arbitrary block μ of a regularly packed brick mortar system (see Fig. 1(a)) and let its centroid be $\boldsymbol{x}^{\mu}$. The pair of neighbors located in the γ^{th} direction, $\boldsymbol{r}^{\gamma\pm}$, are denoted as $\gamma\pm$, and let their centroids be $\boldsymbol{x}^{\mu}+2\boldsymbol{r}^{\gamma\pm}$. Note that $\boldsymbol{r}^{\gamma\pm}$ denote the relative position vectors of the centroid of the contact areas with the neighbors $\gamma\pm$. Let $\boldsymbol{n}^{\gamma}$, $\boldsymbol{t}^{\gamma}$ and $\boldsymbol{s}^{\gamma}$ be an orthonormal coordinate system on contact area with the neighboring block in $\boldsymbol{r}^{\gamma+}$ direction (see Fig. 1(b)). Let the dimension of this rectangular contact area be $2b_t^{\gamma}\times 2b_s^{\gamma}$. Let (x_t,x_s) be an arbitrary point on this contact area, with respect to this local coordinate system.

Assume that the bricks are rigid and undergo infinitesimally small translations and rotations. Let the translation and rotation of μ^{th} block be $\boldsymbol{u}^{\mu}$ and $\boldsymbol{\theta}^{\mu}$, while those of neighbors are $\boldsymbol{u}^{\gamma\pm}$ and $\boldsymbol{\theta}^{\gamma\pm}$. The corresponding relative displacement at the point (x_t,x_s) is

$$\boldsymbol{L}^{\mu\gamma+} = \left(\boldsymbol{u}^{\gamma+}-\boldsymbol{u}^{\mu}\right)-\left(\boldsymbol{\theta}^{\gamma+}+\boldsymbol{\theta}^{\mu}\right)\times\boldsymbol{r}^{\gamma+}+\left(\boldsymbol{\theta}^{\gamma+}-\boldsymbol{\theta}^{\mu}\right)\times\left(x_t\boldsymbol{t}^{\gamma+}+x_s\boldsymbol{s}^{\gamma+}\right).$$

If k and h are the normal and tangential spring constants, respectively, the elastic energy stored in the spring due to the relative deformation $\boldsymbol{L}^{\gamma+}$ is

$$V^{\mu\gamma+} = \frac{1}{2}\int_{-b_s^{\gamma}}^{b_s^{\gamma}}\int_{-b_t^{\gamma}}^{b_t^{\gamma}} k\left(\boldsymbol{n}^{\gamma+}\cdot\boldsymbol{L}^{\mu\gamma+}\right)^2+h\left\{\left(\boldsymbol{t}^{\gamma+}\cdot\boldsymbol{L}^{\mu\gamma+}\right)^2+\left(\boldsymbol{s}^{\gamma+}\cdot\boldsymbol{L}^{\mu\gamma+}\right)^2\right\}\mathrm{d}x_t\mathrm{d}x_s,$$

and the Lagrangian for the whole discrete system is

$$\mathcal{L} = \sum_{\mu}\left(\frac{1}{2}m\dot{\boldsymbol{u}}^{\mu}\cdot\dot{\boldsymbol{u}}^{\mu}+\frac{1}{2}\dot{\boldsymbol{\theta}}^{\mu}\cdot\boldsymbol{I}\cdot\dot{\boldsymbol{\theta}}^{\mu}-V^{\mu}\right), \tag{1}$$

where $V^{\mu}=\frac{1}{2}\sum_{\gamma}(V^{\mu\gamma+}+V^{\mu\gamma-})$. m and $\boldsymbol{I}$ are the mass and inertia tensor of each block.

Applying the Hamilton's principal of stationary action, $\delta\int\mathcal{L}\mathrm{d}t=0$, we can obtain the following governing equations of motion for the discrete system

$$\begin{aligned} m\ddot{\boldsymbol{u}}^{\mu} &= \sum_{\gamma}\boldsymbol{K}^{\mu\gamma}\cdot\left(\boldsymbol{u}^{\gamma+}-2\boldsymbol{u}^{\mu}+\boldsymbol{u}^{\gamma-}\right)-\hat{\boldsymbol{K}}^{\mu\gamma}\cdot\left(\boldsymbol{\theta}^{\gamma+}-\boldsymbol{\theta}^{\gamma-}\right) \\ \boldsymbol{I}\cdot\ddot{\boldsymbol{\theta}}^{\mu} &= \sum_{\gamma}\left(\hat{\boldsymbol{K}}^{\mu\gamma}\right)^{\mathrm{T}}\cdot\left(\boldsymbol{u}^{\gamma+}-\boldsymbol{u}^{\gamma-}\right)-\overline{\boldsymbol{K}}^{\mu\gamma}\cdot\left(\boldsymbol{\theta}^{\gamma+}+2\boldsymbol{\theta}^{\mu}+\boldsymbol{\theta}^{\gamma-}\right)+\overline{\overline{\boldsymbol{K}}}^{\mu\gamma}\cdot\left(\boldsymbol{\theta}^{\gamma+}-2\boldsymbol{\theta}^{\mu}+\boldsymbol{\theta}^{\gamma-}\right), \end{aligned} \tag{2}$$

where

$$
\begin{aligned}
\boldsymbol{K}^{\mu\gamma} &= 4b_t^\gamma b_s^\gamma (k\boldsymbol{n}^\gamma\otimes\boldsymbol{n}^\gamma + h\boldsymbol{t}^\gamma\otimes\boldsymbol{t}^\gamma + h\boldsymbol{s}^\gamma\otimes\boldsymbol{s}^\gamma) \\
\hat{\boldsymbol{K}}^{\mu\gamma} &= 4b_t^\gamma b_s^\gamma \{k\boldsymbol{n}^\gamma\otimes(\boldsymbol{r}^\gamma\times\boldsymbol{n}^\gamma) + h\boldsymbol{t}^\gamma\otimes(\boldsymbol{r}^\gamma\times\boldsymbol{t}^\gamma) + h\boldsymbol{s}^\gamma\otimes(\boldsymbol{r}^\gamma\times\boldsymbol{s}^\gamma)\} \\
\overline{\boldsymbol{K}}^{\mu\gamma} &= 4b_t^\gamma b_s^\gamma \{k(\boldsymbol{r}^\gamma\times\boldsymbol{n}^\gamma)\otimes(\boldsymbol{r}^\gamma\times\boldsymbol{n}^\gamma) + h(\boldsymbol{r}^\gamma\times\boldsymbol{t}^\gamma)\otimes(\boldsymbol{r}^\gamma\times\boldsymbol{t}^\gamma) + h(\boldsymbol{r}^\gamma\times\boldsymbol{s}^\gamma)\otimes(\boldsymbol{r}^\gamma\times\boldsymbol{s}^\gamma)\} \\
\overline{\overline{\boldsymbol{K}}}^{\mu\gamma} &= \frac{4}{3}\left\{h\left(b_t^\gamma b_s^{\gamma 3} + b_t^{\gamma 3} b_s^\gamma\right)\boldsymbol{n}^\gamma\otimes\boldsymbol{n}^\gamma + kb_t^\gamma b_s^{\gamma 3}\boldsymbol{t}^\gamma\otimes\boldsymbol{t}^\gamma + kb_t^{\gamma 3} b_s^\gamma \boldsymbol{s}^\gamma\otimes\boldsymbol{s}^\gamma\right\}
\end{aligned}
$$

For the sake of brevity, γ denotes $\gamma+$ in the above set of equations. It is straight forward to obtain expressions for $\gamma-$ using the following relations: $\boldsymbol{K}^{\mu\gamma+}=\boldsymbol{K}^{\mu\gamma-}$; $\hat{\boldsymbol{K}}^{\mu\gamma+}=-\hat{\boldsymbol{K}}^{\mu\gamma-}$; $\overline{\boldsymbol{K}}^{\mu\gamma+}=\overline{\boldsymbol{K}}^{\mu\gamma-}$; and $\overline{\overline{\boldsymbol{K}}}^{\mu\gamma+}=\overline{\overline{\boldsymbol{K}}}^{\mu\gamma-}$. The set of equations for discrete system given in Eq. (2) can be used to simulate a brick structure as a mass spring system. Though the elastic wave characteristics for given brick mortar properties can be obtained by analyzing the results of such simulations, what is desired for design and verification purposes is the predictability of wave characteristics for arbitrary material properties.

2.2 Equivalent continuum forms

The derivations of the different continuum forms presented in this paper are motivated by Hori et al.'s work on Continuumnization. Hence we first briefly present the outline of their formulation of continuum form, followed by the newly proposed Taylor series approach. Both the approaches assume the presence of smooth vector fields $\boldsymbol{u}$ and $\boldsymbol{\theta}$ which satisfy $\boldsymbol{u}(\boldsymbol{x}^\mu)=\boldsymbol{u}^\mu$ and $\boldsymbol{\theta}(\boldsymbol{x}^\mu)=\boldsymbol{\theta}^\mu$, and make different approximations to the discrete terms $\boldsymbol{u}^{\gamma\pm}-\boldsymbol{u}^\mu$ and $\boldsymbol{\theta}^{\gamma\pm}\pm\boldsymbol{\theta}^\mu$ of Eq. 2.

2.2.1 Continuumnization

In their original work on continuumnization, Hori et al. expressed the discrete terms $\boldsymbol{u}^{\gamma\pm}-\boldsymbol{u}^\mu$ and $\boldsymbol{\theta}^{\gamma\pm}-\boldsymbol{\theta}^\mu$ with differential operators considering the limits $\lim_{\|\boldsymbol{r}^\gamma\|\to 0}\frac{\boldsymbol{u}^{\gamma\pm}-\boldsymbol{u}^\mu}{\|\boldsymbol{r}^\gamma\|}\approx \pm\boldsymbol{r}^\gamma\cdot\nabla\boldsymbol{u}$ and $\lim_{\|\boldsymbol{r}^\gamma\|\to 0}\frac{\boldsymbol{\theta}^{\gamma\pm}-\boldsymbol{\theta}^\mu}{\|\boldsymbol{r}^\gamma\|}\approx\pm\boldsymbol{r}^\gamma\cdot\nabla\boldsymbol{\theta}$. As it will be shown in section 2.2.3, an equivalent continuum form can be obtained by substituting these approximations to Eq. 2.

2.2.2 Taylor series

Instead of using the limiting process, here we use Taylor series expansion to obtain continuous approximations for discrete terms $\boldsymbol{u}^{\gamma\pm}-\boldsymbol{u}^\mu$ and $\boldsymbol{\theta}^{\gamma\pm}-\boldsymbol{\theta}^\mu$. As an example, $\boldsymbol{u}^{\gamma\pm}$ can be approximated as

$$
\boldsymbol{u}^{\gamma\pm} \approx \boldsymbol{u}^\mu \pm 2r_i\left[\frac{\partial\boldsymbol{u}}{\partial x_i}\right]_{\boldsymbol{x}^\mu} + 2r_ir_j\left[\frac{\partial^2\boldsymbol{u}}{\partial x_i\partial x_j}\right]_{\boldsymbol{x}^\mu} \pm \frac{2^3 r_ir_jr_k}{3!}\left[\frac{\partial^3\boldsymbol{u}(\boldsymbol{x})}{\partial x_i\partial x_j\partial x_k}\right]_{\boldsymbol{x}^\mu} + \ldots \qquad (3)
$$

Based on the above expression, we can approximate $(\boldsymbol{u}^{\gamma+}\pm\boldsymbol{u}^{\gamma-})$ and $(\boldsymbol{u}^{\gamma+}-\boldsymbol{u}^{\gamma-})$ as

$$\begin{aligned}
\boldsymbol{u}^{\gamma+}+\boldsymbol{u}^{\gamma-} &\approx 2\boldsymbol{u}^{\mu}+\frac{2^3 r_i r_j}{2!}\left[\frac{\partial^2 \boldsymbol{u}(\boldsymbol{x})}{\partial x_i \partial x_j}\right]_{\boldsymbol{x}^\mu}+\frac{2^5 r_i r_j r_k r_l}{4!}\left[\frac{\partial^4 \boldsymbol{u}(\boldsymbol{x})}{\partial x_i \partial x_j \partial x_k \partial x_l}\right]_{\boldsymbol{x}^\mu}+\ldots \\
\boldsymbol{u}^{\gamma+}-\boldsymbol{u}^{\gamma-} &\approx \left[\frac{\partial \boldsymbol{u}(\boldsymbol{x})}{\partial x_i}\right]_{\boldsymbol{x}^\mu} 2^2 r_i+\frac{2^4 r_i r_j r_k}{3!}\left[\frac{\partial^3 \boldsymbol{u}(\boldsymbol{x})}{\partial x_i \partial x_j \partial x_k}\right]_{\boldsymbol{x}^\mu}+\ldots
\end{aligned} \tag{4}$$

Similarly, it is straight forward to express $(\boldsymbol{\theta}^{\gamma+}\pm\boldsymbol{\theta}^{\gamma-})$. The Taylor series approach uses the above expressions for approximating the discrete terms $(\boldsymbol{u}^{\gamma+}\pm\boldsymbol{u}^{\gamma-})$ and $(\boldsymbol{\theta}^{\gamma+}\pm\boldsymbol{\theta}^{\gamma-})$ in terms of continuous vector fields $\boldsymbol{u}(\boldsymbol{x})$ and $\boldsymbol{\theta}(\boldsymbol{x})$.

2.2.3 Equivalent continuum forms of discrete governing equations

Neglecting all the third or higher order derivatives terms of Eq. 4 and substituting to Eq. 2, we can obtain the following second order accurate continuum form for the idealized discrete brick mortar system.

$$\begin{aligned}
\frac{m}{V_b}\ddot{\boldsymbol{u}} &= \nabla\cdot(\boldsymbol{c}:\nabla\boldsymbol{u})-\boldsymbol{q}:\nabla\boldsymbol{\theta} \\
\frac{1}{V_b}\boldsymbol{I}\cdot\ddot{\boldsymbol{\theta}} &= \boldsymbol{q}^{\mathrm{T}}:\nabla\boldsymbol{u}-\boldsymbol{d}\cdot\boldsymbol{\theta}+\nabla\cdot(\boldsymbol{v}:\nabla\boldsymbol{\theta}),
\end{aligned} \tag{5}$$

where V_b is the volume of a block. $\boldsymbol{c}$, $\boldsymbol{q}$, $\boldsymbol{d}$, and $\boldsymbol{v}$ are 4^{th}, 3^{rd}, 2^{nd}, and 4^{th}-order tensors composed of material and geometric (i.e. block geometry and packing) properties. Explicit expressions for these tensors for the second order Taylor series based continuum form are

$$\begin{aligned}
\boldsymbol{c} &= \frac{16}{V_b}\sum_{\gamma} b_t^{\gamma} b_s^{\gamma}\left(k\boldsymbol{r}^{\gamma}\otimes\boldsymbol{n}^{\gamma}\otimes\boldsymbol{r}^{\gamma}\otimes\boldsymbol{n}^{\gamma}+h\boldsymbol{r}^{\gamma}\otimes\boldsymbol{t}^{\gamma}\otimes\boldsymbol{r}^{\gamma}\otimes\boldsymbol{t}^{\gamma}+h\boldsymbol{r}^{\gamma}\otimes\boldsymbol{s}^{\gamma}\otimes\boldsymbol{r}^{\gamma}\otimes\boldsymbol{s}^{\gamma}\right) \\
\boldsymbol{q} &= \frac{16}{V_b}\sum_{\gamma} b_t^{\gamma} b_s^{\gamma}\left\{k\boldsymbol{n}^{\gamma}\otimes\boldsymbol{r}^{\gamma}\otimes(\boldsymbol{r}^{\gamma}\times\boldsymbol{n}^{\gamma})+h\boldsymbol{t}^{\gamma}\otimes\boldsymbol{r}^{\gamma}\otimes(\boldsymbol{r}^{\gamma}\times\boldsymbol{t}^{\gamma})+h\boldsymbol{s}^{\gamma}\otimes\boldsymbol{r}^{\gamma}\otimes(\boldsymbol{r}^{\gamma}\times\boldsymbol{s}^{\gamma})\right\} \\
\boldsymbol{d} &= \frac{16}{V_b}\sum_{\gamma} b_t^{\gamma} b_s^{\gamma}\left\{k(\boldsymbol{r}^{\gamma}\times\boldsymbol{n}^{\gamma})\otimes(\boldsymbol{r}^{\gamma}\times\boldsymbol{n}^{\gamma})+h(\boldsymbol{r}^{\gamma}\times\boldsymbol{t}^{\gamma})\otimes(\boldsymbol{r}^{\gamma}\times\boldsymbol{t}^{\gamma})+h(\boldsymbol{r}^{\gamma}\times\boldsymbol{s}^{\gamma})\otimes(\boldsymbol{r}^{\gamma}\times\boldsymbol{s}^{\gamma})\right\} \\
\boldsymbol{v} &= \frac{16}{3V_b}\sum_{\gamma} b_t^{\gamma} b_s^{\gamma}\boldsymbol{r}^{\gamma}\otimes\Big\{\Big\{h\left(b_s^{\gamma 2}+b_t^{\gamma 2}\right)\boldsymbol{n}^{\gamma}\otimes\boldsymbol{r}^{\gamma}\otimes\boldsymbol{n}^{\gamma}+kb_s^{\gamma 2}\boldsymbol{t}^{\gamma}\otimes\boldsymbol{r}^{\gamma}\otimes\boldsymbol{t}^{\gamma}+kb_t^{\gamma 2}\boldsymbol{s}^{\gamma}\otimes\boldsymbol{r}^{\gamma}\otimes\boldsymbol{s}^{\gamma}\Big\} \\
&\quad -3\left\{k(\boldsymbol{r}^{\gamma}\times\boldsymbol{n}^{\gamma})\otimes\boldsymbol{r}^{\gamma}\otimes(\boldsymbol{r}^{\gamma}\times\boldsymbol{n}^{\gamma})+h\left((\boldsymbol{r}^{\gamma}\times\boldsymbol{t}^{\gamma})\otimes\boldsymbol{r}^{\gamma}\otimes(\boldsymbol{r}^{\gamma}\times\boldsymbol{t}^{\gamma})+(\boldsymbol{r}^{\gamma}\times\boldsymbol{s}^{\gamma})\otimes\boldsymbol{r}^{\gamma}\otimes(\boldsymbol{r}^{\gamma}\times\boldsymbol{s}^{\gamma})\right)\right\}\Big\}
\end{aligned}$$

In the original work by Hori et al.[1], a first order approximation is made for the term $(\boldsymbol{\theta}^{\gamma+}+2\boldsymbol{\theta}^{\mu}+\boldsymbol{\theta}^{\gamma-})\approx 4\boldsymbol{\theta}(\boldsymbol{x}^{\mu})$, instead of $4\boldsymbol{\theta}+4r_i r_j\left[\frac{\partial^2\boldsymbol{\theta}(\boldsymbol{x})}{\partial x_i\partial x_j}\right]_{\boldsymbol{x}^\mu}$ used in the above second order Taylor series approximation. Consequently, the term $\nabla\cdot(\boldsymbol{v}:\nabla\boldsymbol{\theta})$ of Eq. 5 is not present in the continuum form of governing equations from continuumnization.

Table 1: Wave velocities and corresponding modes $\{u_1,u_2,\theta_3\}$ for θ_ξ=90° and θ_ξ=0°. $\zeta=a_2/a_1$ and $\eta=h/k$

wave type	θ_ξ=90°		θ_ξ=0°	
	phase velocity	mode shape	phase velocity	mode shape
p	$\sqrt{\frac{2ka_2}{\rho}}$	$\{0,1,0\}$	$\sqrt{\frac{ka_2(\eta+4\zeta)}{2\rho\zeta^2}}$	$\{1,0,0\}$
s	$\sqrt{\frac{2ka_2\eta(1+4\eta\zeta)}{\rho(1+4\eta\zeta+4\eta\zeta^2)}}$	$\left\{1,0,-\frac{4\eta\zeta^2\xi\mathrm{i}}{1+4\eta\zeta+4\eta\zeta^2}\right\}$	$\sqrt{\frac{2ka_2\eta(1+4\eta\zeta)}{\rho(1+4\eta\zeta+4\eta\zeta^2)}}$	$\left\{0,1,-\frac{(1+4\eta\zeta)\xi\mathrm{i}}{1+4\eta\zeta+4\eta\zeta^2}\right\}$
r	-	$\{0,0,1\}$	-	$\{0,0,1\}$

While the above second order Taylor expansion based continuum form was independently developed by the authors, Stefanou et al.[2] also have proposed similar idea of obtaining equivalent continuum form of regularly arranged brick structures based on second order Taylor expansion.

2.2.4 Prediction of elastic wave characteristics

A major advantage of Eq.(5) is that it makes it possible to analytically study the dynamic characteristics of the approximated discrete system. As an example, consider the two dimensional single layered brick wall shown in Fig.2. For this given packing, we can evaluate the four tensors, $\boldsymbol{c}$, $\boldsymbol{q}$, $\boldsymbol{d}$, and $\boldsymbol{v}$, and obtain the equivalent continuum form of equations of motion (i.e. Eq.(5)). Taking the Fourier transform of the resulting equations, with the kernel of $e^{\imath(\boldsymbol{\xi}\cdot\boldsymbol{x}-\omega t)}$, where $\boldsymbol{\xi}=\xi\{\cos\theta_\xi,\sin\theta_\xi\}$, and solving the resulting characteristic equations, the relations between the wave frequencies and wave numbers for in-plane deformations can be obtained. Since the system is anisotropic, the wave velocities depend on the direction of the propagating wave. Table 1 shows the p-, s- and r- wave charateristics based on the continuum form with the second order Taylor expansion.

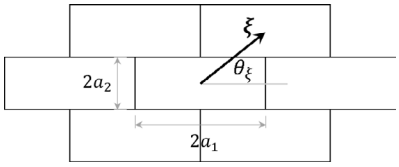

Figure 2: A single layered 2 dimensional brick arrangement.

Though r-wave speed is undefined, we can obtain following expression for frequency of rotational mode

$$\omega_{\mathrm{spin}}=\sqrt{\frac{3ka_1^2+12ha_1a_2+12ha_2^2}{2\rho a_1^2a_2+2\rho a_2^3}}. \tag{6}$$

2.2.5 Prediction of elastic wave characteristics based on an arbitrary order approximation

In the section 2.2.3, we used only the terms up to the second order derivatives in Eq.(4). It surely is odd to consider all the infinite terms of the Taylor expansion in approximating variables. However lets consider all the terms of Taylor series expansion and obtain a continuum form, which is obviously too complicated for any practical use. The presence of some series solutions make it is possible to obtain a quite compact characteristic equation when all the infinite terms of Eq.(4) are used.

With a little bit of mathematical manipulations, the following two relations for the Fourier transform of Eq.(4) can be established; note that all the infinite terms in the Taylor series are included.

$$\begin{aligned}\int \left(\boldsymbol{u}^{\gamma+}+\boldsymbol{u}^{\gamma-}\right)e^{\imath(\boldsymbol{\xi}\cdot\boldsymbol{x}-\omega t)}\mathrm{d}\boldsymbol{x}\mathrm{d}t &\approx 2\left(1-2\sin^2(\boldsymbol{\xi}\cdot\boldsymbol{r}^{\gamma})\right)\hat{\boldsymbol{u}}\\ \int (\boldsymbol{u}^{\gamma+}-\boldsymbol{u}^{\gamma-})e^{\imath(\boldsymbol{\xi}\cdot\boldsymbol{x}-\omega t)}\mathrm{d}\boldsymbol{x}\mathrm{d}t &\approx 2\imath\{\sin(2\boldsymbol{\xi}\cdot\boldsymbol{r}^{\gamma})\}\hat{\boldsymbol{u}}\end{aligned} \tag{7}$$

$\hat{\boldsymbol{u}}$ and $\hat{\boldsymbol{\theta}}$ are the Fourier transform of $\boldsymbol{u}$ and $\boldsymbol{\theta}$ with respect to the kernel $e^{\imath(\boldsymbol{\xi}\cdot\boldsymbol{x}-\omega t)}$. Now, approximating the discrete terms $(\boldsymbol{u}^{\gamma+}\pm\boldsymbol{u}^{\gamma-})$ and $(\boldsymbol{\theta}^{\gamma+}\pm\boldsymbol{\theta}^{\gamma-})$ of Eq.(4) with the full Taylor series and taking the Fourier transform, we can obtain the following set of equations.

$$0 = \det\begin{bmatrix} -\omega^2\boldsymbol{M}+\sum_{\gamma}4\sin^2(\boldsymbol{\xi}\cdot\boldsymbol{r}^{\gamma})\boldsymbol{K}^{\mu\gamma} & 2\imath\sum_{\gamma}\sin(2\boldsymbol{\xi}\cdot\boldsymbol{r})\hat{\boldsymbol{K}}^{\mu\gamma} \\ -2\imath\sum_{\gamma}\sin(2\boldsymbol{\xi}\cdot\boldsymbol{r}^{\gamma})\left(\hat{\boldsymbol{K}}^{\mu\gamma}\right)^{\mathrm{T}} & -\omega^2\boldsymbol{I}+4\sum_{\gamma}\left(\cos^2(\boldsymbol{\xi}\cdot\boldsymbol{r}^{\gamma})\overline{\boldsymbol{K}}^{\mu\gamma}+\sin^2(\boldsymbol{\xi}\cdot\boldsymbol{r}^{\gamma})\overline{\overline{\boldsymbol{K}}}^{\mu\gamma}\right)\end{bmatrix}$$

$\boldsymbol{M}=m\mathbf{1}$ is the mass matrix and $\boldsymbol{I}$ is the inertia tensor of a brick; $\mathbf{1}$ is the identity matrix.

Though the above is too complicated to solve for analytical relations between frequencies and wave numbers, ω and $\boldsymbol{\xi}$, we can numerically solve it to find relation between ω and $\boldsymbol{\xi}$. As it will be shown in the next section, the wave properties predicted with this characteristic function is valid for much wider range of wave numbers, compared to above obtained predictions from continuumnization and second order Taylor series approximation.

3 VERIFICATION OF THE PREDICTED WAVE PROPERTIES

To verify the elastic wave characteristics predicted in sections 2.2.4 and 2.2.5 and identify the applicable range of these predictions, we compared the predicted properties with the results obtained from a Rigid Body Spring Model (RBSM) simulation. The details of this comparison is presented in this section.

3.1 Basic problem settings

A brick wall of width 20.3m and height 13.0m shown in Fig.3 was used for the RBSM simulations. The bricks are 60mm in width, 30mm in height, and 40mm in thickness. The density of each block is assumed to be 1850kg/m^3. k and h, are determined as 5.12×10^{11}N/m^3 and 2.22×10^{11}N/m^3, respectively.

For the sake of simplicity, 2D settings was assumed and the domain was excited with an in-plane wave at center of the domain. We considered 3 cases with different inputs. First and second cases were with transnational waves of vertical and horizontal excitation. The third case was with a rotational wave input. In all the cases, the wave form shown in Fig. 3b was used.

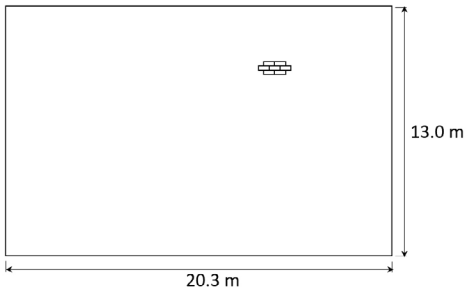

(a) Domain

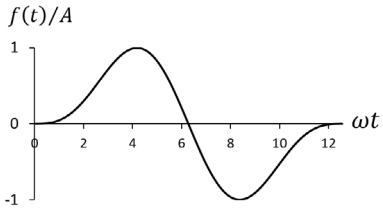

(b) Input wave $f(t)=\frac{4}{3\sqrt{3}}A\left(\sin\frac{\omega t}{2}-\frac{1}{2}\sin\omega t\right)$

Figure 3: Domain and the wave form used in the numerical experiments.

A and ω are the amplitude and circular frequency of the input. For vertical and horizontal inputs A=2mm while A=0.035 radians for the rotational input. To obtain narrow wave fronts, so that peaks and valleys of waves are clearly visible, input circular frequency ω is set 1.57×10^4radian/s for vertical and horizontal input, and 2.11×10^5radian/s for rotational input.

In order to obtain accurate results, we used a second order velocity Verlet algorithm with $1\mu s$ time step for time integration. As an indirect check of accuracy of the simulation, energy and momentum of the whole system were monitored. Near perfect preservation of energy and momentum was observed, indicating that the simulations were accurate.

3.2 Comparison of translational waves

The color contours of Fig. 4(a) and (b) show the distribution of translational wave amplitudes at time 2ms. The two black color curves indicate the analytically predicted wave fronts based on the continuum form from the second order Taylor expansion presented in the section 2.2.3.

3.2.1 P-wave

As is seen, the analytically predicted p-wave fronts are in good agreement with numerical results in the regions indicated with letter A. The wave profiles along section P-P, shown in the left side pair of Fig.5 clearly indicate that the analytical predictions are in good agreement with the numerical results. In Fig.4(a), since the input wave is oriented in vertical direction, the p-wave amplitude is highest in up and down directions, while it is extremely low in other directions. This is why no p-wave fronts are visible in the numerical results except in up and down directions in Fig.4(a), and left and right directions in Fig.4(b).

3.2.2 S-wave

Also, the Fig. 4(a) and (b) show that the theoretically predicated s-wave fronts are also in good agreement with that of numerical results in the regions marked with letter B. The right hand side pair in Fig.5 provides clear evidences to support this claim. Amplitude of the main s-wave is weak in most directions, except orthogonal to the direction of excitation. This is why there seems to be a significant mismatch between numerical and analytical wave fronts in regions except B.

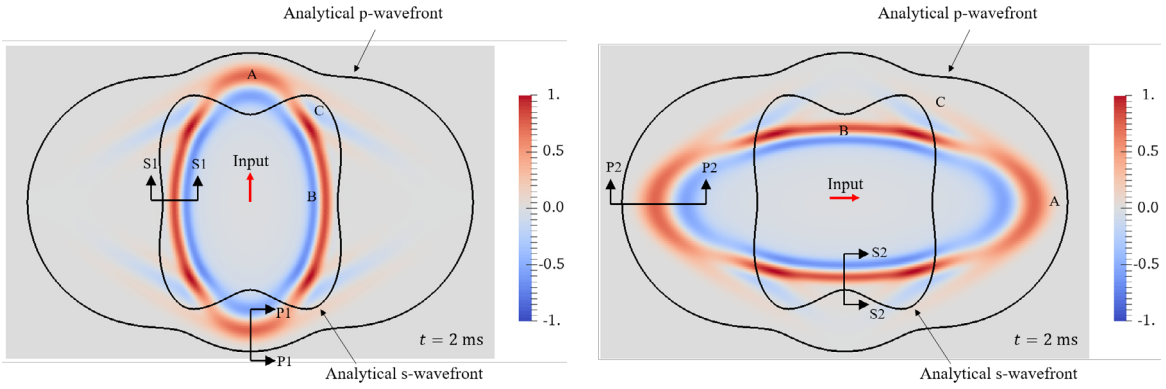

(a) with vertical input (b) with horizontal input

Figure 4: Comparison of predicted p- and s-wave fronts with those of numerical results, at 2 ms. The colors indicate the amplitude of translational waves.

3.3 Comparison of rotational waves

Fig. 6 shows the distribution of the amplitudes of rotational waves (r-wave) generated by the rotational wave input, at 2 ms. Unlike the translational wave inputs, dispersion of the rotational wave occurs. In order to check the accuracy of predictions, we compared the circular frequency ω versus the normalized wave number ξa_i where a_1 and a_2 are the

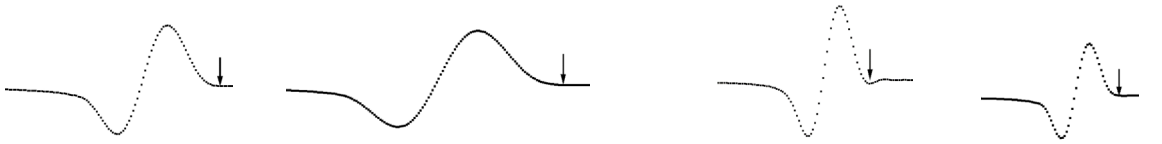

(c) along sections P-P (f) along sections S-S

Figure 5: P-wave profiles along sections P-P (left pair) and s-wave profiles along sections S-S (right pair), at 2 ms. Arrows indicates the analytically predicted wave front.

half of the dimensions of a brick (see Fig.2). The ω versus ξa_i relations of the numerical results are obtained by Fast Fourier Transform (FFT) with respect to space and time. FFT was conducted for two narrow vertical and horizontal spatial domains shown with yellow lines in Fig.6.

The results of the double FFTs are shown in Fig.7. As seen, in addition to the r-wave, small amplitude p- and s-waves are also present. This gives us a good opportunity to make a further check the accuracy of predicted p- and s- wave characteristics.

Figure 7 (a) and (b) compare the predictions with continuumnization by Hori et al.[1]. The analytical prediction of rotational frequency is in agreement only in a small neighborhood of $|\xi a_1|=|\xi a_2|=0$, and it rapidly diverges when move away from this small neighborhood. This is not surprising since continnumnization uses only the 0^{th}-order approximation $(\boldsymbol{\theta}^{\gamma+}+2\boldsymbol{\theta}^{\mu}+\boldsymbol{\theta}^{\gamma-})\approx 4\boldsymbol{\theta}^{\mu}$.

As show in Fig. 7 (c) and (d), the predictions with the second order Taylor expansion (see section 2.2.3) are in good agreement with the numerical solution within the range $|\xi a_i|<0.5$. P-, s- and r-wave predictions based on this continuum form are valid for the wavelengths grater than 7 times the size of bricks.

The advantage of the continuum form obtained with the full Taylor series is clearly seen in Fig. 7 (e) and (f). Analytical predictions for s- p- and r-waves are in near perfect agreement with the numerical results for a whole range of wave numbers considered. Note that we limited our analysis to the range $\xi a_i \leq 1.5$ since it corresponds to the shortest meaningful wavelength for the considered problem; $\xi a_i \leq 1.5$ includes wavelengths two times larger than the respective dimensions of a brick.

4 CONCLUDING REMARKS

Three equivalent continuum forms are developed for regularly packed brick structures and utilized to predict the elastic wave characteristics. The predicted p- and s-waves characteristics based on continnumnization and second order Taylor expansion are accurate for wavelengths greater than 7 times the size of bricks. In case of r-wave, while the predictions of second order Taylor expansion approach is accurate in the same wavelength range, that of continnumnization is limited to narrow range of wavelengths. The full Taylor series based continuum form can predict the elastic wave properties to a remarkable accuracy

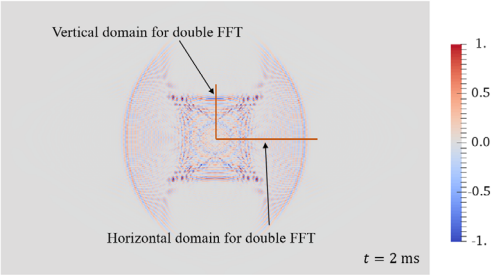

Figure 6: Magnitude of the rotational waves at 2 ms, generated by rotational wave input. Two lines indicate the domains used for double FFT.

for the whole range of wave numbers. These predictions will be useful in verification of numerical simulations and engineering applications like non-destructive testing, vibration control, structural design, etc. For the ordinary design purposes the predictions based on continnumnization or second order Taylor expansion is sufficient, while the full Taylor series model will be useful in physics applications involving high frequencies. Further, it is straight forward to develop Finite Element extensions based on these continuum forms for analyzing brick structures.

REFERENCES

[1] Hori, M., Wijerathne, L., Chen, J. and Ichimura, T.: Continuumnization of regularly arranged rigid bodies, *Journal of JSCE*,Vol. 4, pp. 38-45, 2016.

[2] Stefanou, I., Sulem, J. and Vardoulakis, I.:Three-dimensional cosserat homogenization of masonry structures: elasticity, *Acta Geotechnica*, *Springer Verlag*, Vol. 3(1), pp.71-83, 2008.

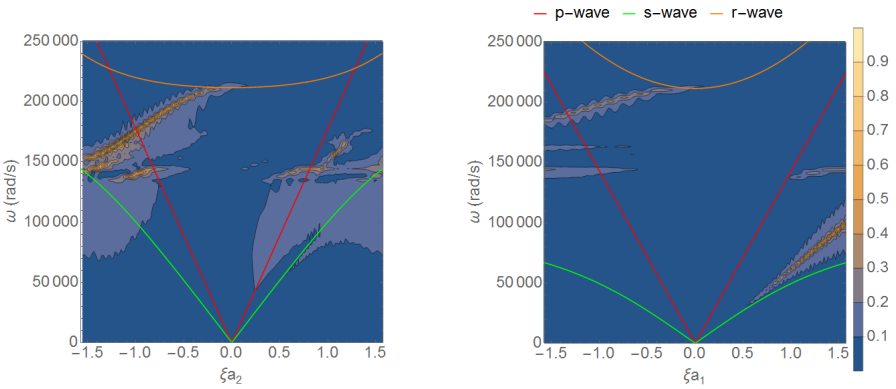

(a) Along the vertical domain (b) Along the horizontal domain

Continnumnization

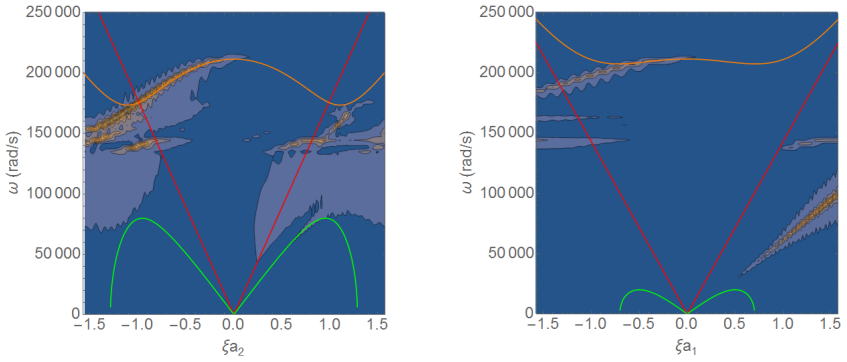

(c) Along the vertical domain (d) Along the horizontal domain

Second order Taylor series

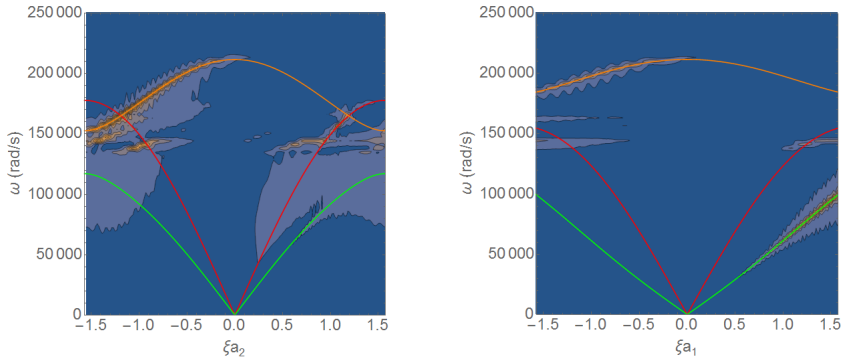

(e) Along the vertical domain (f) Along the horizontal domain

Full Taylor series

Figure 7: Comparison of numerical results and the analytical predictions based on different continuum forms. Contour plots show the numerically obtained amplitude of ω vs. ξa_i relation. The curves shows the analytical prediction for p-, s- and rotational waves.